Hermitian topologies originating from non-Hermitian braidings

W. B. Rui,* Y. X. Zhao,† and Z. D. Wang‡

Department of Physics and HKU-UCAS Joint Institute for Theoretical and Computational Physics at Hong Kong, The University of Hong Kong, Pokfulam Road, Hong Kong, China

and HK Institute of Quantum Science & Technology, The University of Hong Kong, Pokfulam Road, Hong Kong, China

(Received 1 June 2022; revised 5 August 2023; accepted 19 September 2023; published 3 October 2023)

The complex energy bands of non-Hermitian systems braid in momentum space even in one dimension. Here, we reveal that the non-Hermitian braiding underlies the Hermitian topological physics with chiral symmetry under a general framework that unifies Hermitian and non-Hermitian systems. Particularly, we derive an elegant identity that equates the linking number between the knots of braiding non-Hermitian bands and the zero-energy loop to the topological invariant of chiral-symmetric topological phases in one dimension. Moreover, we find an exotic class of phase transitions arising from the critical point transforming different knot structures of the non-Hermitian braiding, which are not included in the conventional Hermitian topological phase transition theory. Nevertheless, we show the bulk-boundary correspondence between the bulk non-Hermitian braiding and boundary zero modes of the Hermitian topological insulators. Finally, we construct typical topological phases with non-Hermitian braidings, which can be readily realized by artificial crystals.

DOI: 10.1103/PhysRevB.108.165105

I. INTRODUCTION

The concept of topology captures properties unchanged under continuous deformations. It can be pictorially illustrated by knots formed by braids, which cannot be unknotted by continuous stretching. While initially introduced to describe the behavior of anyons [1–3], braiding was recently actively investigated in momentum-space band structures [4–19], where braids appear in various scenes, such as nodal lines in topological semimetals [4–7], the trajectories of Weyl or Dirac points in adiabatic time evolution [8–11], and exceptional rings in non-Hermitian systems [12–15].

Another active trend in recent research is to generalize elements of Hermitian topological phases to non-Hermitian systems [20–34]. Fundamental topological concepts, such as topological invariants, bulk-boundary correspondence, and topological stability, were reconsidered by incorporating non-Hermitian features [30,32–39], such as gain-and-loss processes and exceptional points. This leads to novel topological classifications, and a plethora of non-Hermitian topological phase with exotic non-Hermitian topological phenomena [30,32–53]. Particularly, a massive number of states reside on the boundary in the non-Hermitian skin effect [47–54], rather than a few boundary states for Hermitian topological insulators.

Non-Hermitian physics and braiding are not independent. The energy spectra of non-Hermitian systems are complex numbers, and hence the complex bands can naturally braid in the complex plane even through a one-dimensional (1D) Brillouin zone. This leads to a recent classification of non-Hermitian 1D systems by the knot structures [55–59].

In this paper, we reverse the conventional reasoning by understanding Hermitian topological physics in terms of non-Hermitian braiding in one dimension. *A priori*, there is a formal one-to-one map between a Hermitian Hamiltonian H in class AIII and a non-Hermitian operator Q in the basis specified by the eigenstates of the chiral symmetry. Using the map, we find that a number of fundamentals of Hermitian topology acquire more pictorial understandings from the braiding structure of the non-Hermitian bands. Particularly, we rigorously show that the abstractly defined topological invariant of the Su-Schrieffer-Heeger (SSH) model can be visualized as the linking number between the knots of the complex non-Hermitian bands and the zero-energy loop. Since the left and right zero modes of Q are exactly the zero modes of H with opposite chirality, we see that the end zero modes of the Hermitian insulator can be regarded as consequences of the bulk non-Hermitian braiding. Nevertheless, the braiding rationale can give rise to a novel class of topological phase transitions characterized by the critical points where the knot structure of the non-Hermitian bands transforms, which go beyond the conventional theory of topological phase transitions. Moreover, we construct typical topological phases using our theory, which can be readily realized by artificial crystals.

II. FRAMEWORK

Let us start with a non-Hermitian system described by the Hamiltonian Q. Using Q, a Hermitian Hamiltonian H with chiral symmetry S can be built as

$$H=\begin{pmatrix}0 & Q\\ Q^\dagger & 0\end{pmatrix},\quad S=\begin{pmatrix}\mathbb{I} & 0\\ 0 & -\mathbb{I}\end{pmatrix},\quad SHS^\dagger=-H. \tag{1}$$

*wbrui@hku.hk
†yuxinphy@hku.hk
‡zwang@hku.hk

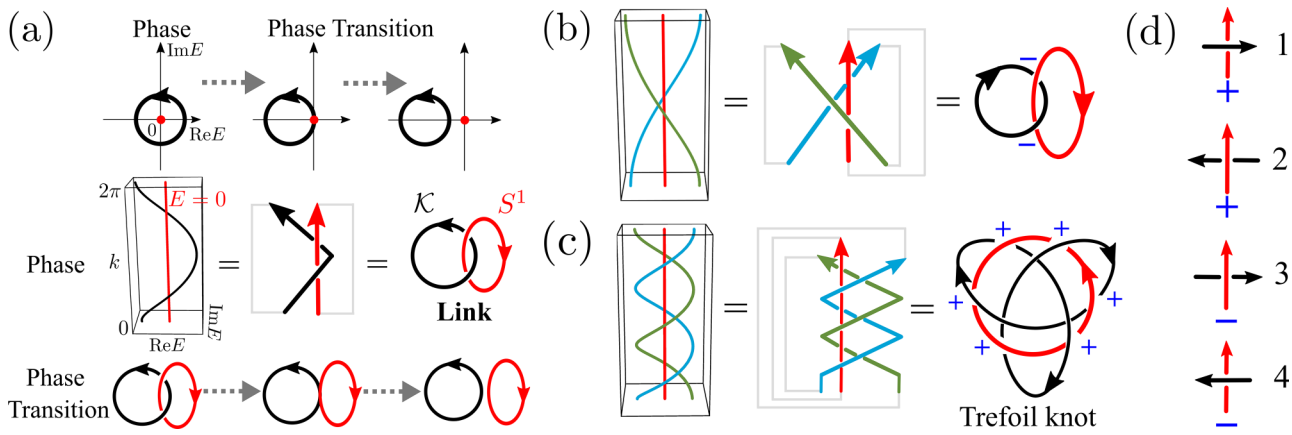

FIG. 1. Non-Hermitian braidings as the origin of Hermitian topological phases. (a) Upper panel: the conventional 2D picture of topological phase and its transition. Middle panel: the single band braids trivially and forms a knot of circle. The 3D picture shows the topological origin as the linking between knot (black) and zero-energy loop (red). Lower panel: 3D picture of unlinking as the phase transition. (b) Knot of circle formed by the braiding of bands. (c) Trefoil knot formed by the braiding of bands. (d) Illustrations of four types of crossings in the algorithm to calculate the topological invariant.

Here † denotes the conjugate transpose and $\mathbb{I}$ the identity matrix. For the eigenequtions $H|\Psi\rangle = E|\Psi\rangle$, the chiral symmetry results in another set of eigenmodes $\{-E, S|\Psi\rangle\}$. Thus, the energy spectrum is symmetric with respect to zero energy.

A key observation is that for zero energy, i.e., $E = 0$, the chiral-symmetric Hermitian H is decoupled to non-Hermitian Q and $Q^\dagger$. Although seemingly minor, we will show that the non-Hermitian topological properties of Q with respect to this zero energy dictate the bulk topology, topological phase transition, and bulk-boundary correspondence of the Hermitian H. Thus, the zero energy serves as a guideline in our study.

Since zero-energy eigenstates of H are at the same time the eigenstates of S, they can be classified as left handed (right handed) according to the eigenvalues $+1$ (-1) of the chiral operator. Introduce $|\Psi\rangle = (\psi_+, \psi_-)^T$ as the eigenstates of H. The zero-energy eigenstates ($|\Psi_\pm\rangle$) of different chiralities are obtained as

$$H|\Psi_\pm\rangle = 0: \quad |\Psi_+\rangle = (\psi_+, 0)^T, |\Psi_-\rangle = (0, \psi_-)^T, \quad (2)$$

which satisfies $S|\Psi_\pm\rangle = \pm|\Psi_\pm\rangle$. Clearly, H shares the same eigenstates with Q and $Q^\dagger$, as

$$E = 0: \quad Q^\dagger\psi_+ = 0, \quad Q\psi_- = 0. \quad (3)$$

Thus, we may regard that the zero-energy modes in chiral-symmetric Hermitian systems originate from the non-Hermitain components. In contrast, non-zero-energy eigenstates of Q can not retain in H [60].

III. ORIGIN OF HERMITIAN TOPOLOGICAL PHASES: BRAIDINGS OF NON-HERMITIAN ENERGY BANDS

We consider Q with no symmetry (non-Hermitian class A) and H with only chiral symmetry (Hermitian class AIII) in Eq. (1) [32,61]. In one dimension (1D), both H and Q are characterized by the winding number of

$$w = \frac{1}{2\pi i}\oint_{\mathrm{BZ}^1} dk \cdot \nabla_k \log\det \mathcal{Q}(k), \quad (4)$$

where k denotes the momentum and $\mathcal{Q}(k)$ the corresponding Hamiltonian in the 1D Brillouin zone (BZ^1) [62,63]. In this regard, $H(k)$ and $Q(k)$ share the same topology and, formerly, correspondences between the two have been established [30,32,64,65]. It turns out the "one-to-one correspondence" [32,64] describing the topological equivalence between the Hermitian topology of H and the point-gap topology [66] of Q is quite useful, and a systematic classification of the point-gap topology of Q using H has been worked out in higher dimensions and in other symmetry classes.

It shall be noted that the "one-to-one correspondence" above is based on the point-gap topology of Q. Recently, however, it has been shown that the non-Hermitian $\mathcal{Q}(k)$ actually has a three-dimensional (3D) braiding topology in the (k, ReE, ImE) space [55–58] as shown in Figs. 1(a)–1(c), which goes beyond the point-gap topology. In view of this, the well-established equivalence relation between Q and H may not be sufficient.

However, the topological invariant in Eq. (4) is not able to capture all the physics, because it is essentially a two-dimensional (2D) quantity, while the braiding structure of $\mathcal{Q}(k)$ lives in three dimensions (3D). Thus, it is necessary to develop a 3D picture to understand the topological origin and further explore the relation between Q and H. In the middle panel of Fig. 1(a), the single band of $\mathcal{Q}(k)$ braids trivially and forms a knot of circle (black) over BZ in 3D, while the zero-energy point forms a closed loop (red). To have a nontrivial phase, the knot ($\mathcal{K}$) and the zero-energy loop (S^1) must form a link. Note that the zero-energy loop S^1 is defined by a constant function $E(k) = 0, \forall\, k \in [0, 2\pi)$, which forms a loop due the periodicity of BZ. Then, the winding number in Eq. (4) actually reflects the linking number between the two,

$$w = \mathrm{Link}(\mathcal{K}, S^1). \quad (5)$$

It is clear now that the topological phase transition, as shown in the lower panel of Fig. 1(a), is triggered by the unlinking process between $\mathcal{K}$ and S^1. This is in contrast with the conventional understanding of the phase transition induced by

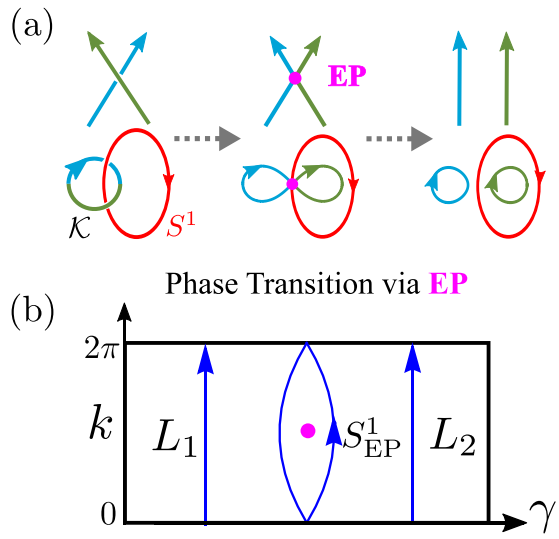

FIG. 2. Phase transition via critical point in non-Hermitian braidings. (a) The transformation of non-Hermitian braiding in $\mathcal{Q}(k)$ via EP. (b) The transformation via EP can induce Hermitian topological phase transition in $\mathcal{H}(k)$.

shifting the energy band away from the zero-energy point, as shown by the upper panel of Fig. 1(a).

The linking number of Eq. (5) goes beyond the previously mentioned correspondence between $\mathcal{H}(k)$ and $\mathcal{Q}(k)$, and can faithfully describe the topological origin of $\mathcal{H}(k)$. This is more evident for general cases of multiband $\mathcal{Q}(k)$. In these cases, the n separable bands of $\mathcal{Q}(k)$ braid with each other [e.g., Figs. 1(b) and 1(c)], and form knots due to the periodicity of BZ. As different braiding structures may correspond to the same point-gap topology, the 2D winding number by Eq. (4), while valid in describing point-gap topology, may be blind to these 3D braiding structures. The 3D linking number, on the other hand, can faithfully tell us that the topological phases of $\mathcal{H}(k)$ originate from the non-Hermitian braidings in $\mathcal{Q}(k)$.

Compared to Eq. (4), the linking number may also simplify the calculation [67] because it can be obtained by just counting the crossings,

$$\mathrm{Link}(\mathcal{K}, S^1) = \frac{n_1 + n_2 - n_3 - n_4}{2}, \tag{6}$$

where n_i denotes the number of four types of crossings, as shown in Fig. 1(d). For instance, by simply counting the crossings, the winding number of the knot of circle in Fig. 1(b) and the Trefoil knot in Fig. 1(c) is obtained as $w = -1$ and $+3$, respectively.

IV. HERMITIAN TOPOLOGICAL PHASE TRANSITION VIA CRITICAL POINT IN NON-HERMITIAN BRAIDINGS

The above discussion of the non-Hermitian braidings as the origin of Hermitian topology leads to our discovery of a different kind of topological phase transitions, which goes beyond the conventional theory of topological phase transitions shown in the first row of Fig. 1(a).

As illustrated by Fig. 2(a), where the two bands braid with each other, the linking number can also be changed by the transformation of the braiding structure. Here, the unlinking between $\mathcal{K}$ and S^1 is realized by the change of braiding of $\mathcal{Q}(k)$. It happens via the critical point where two bands intersect on the zero-energy loop. Such a critical point is a unique non-Hermitian degeneracy, namely, exceptional point (EP) [26,57], which results in the phase transition in $\mathcal{H}(k)$.

Suppose that the phase transition is induced by tuning an extra parameter γ. Then the momentum and this extra parameter form a 2D (k, γ) space, where EP could appear in this 2D space. As shown in Fig. 2(b), $k_{\rm EP}$ denotes the position of EP and $S^1_{\rm EP}$ denotes the loop that encircles $k_{\rm EP}$. To show that EPs can induce phase transitions in Hermitian systems, recall that for order-2 EPs in 2D space, there is an associated topological invariant of vorticity [26,68]

$$v_\pm = -\frac{1}{2\pi}\oint_{S^1_{\rm EP}} d\mathbf{k}\cdot\nabla_{\mathbf{k}}\arg\left[E_+(\mathbf{k}) - E_-(\mathbf{k})\right], \tag{7}$$

where $\pm$ denote the band indices, and $\mathbf{k}$ refers to the combination (k, γ). The vorticity is a non-Hermitian invariant and takes half-integer values $(\mathbb{Z}/2)$ because EP acts as a branch point on the complex-energy plane. Thus, it is essentially different from Hermitian topological invariants.

Notably, it can be proved that EP can alter the winding number of

$$w(\mathbf{k}_{\rm EP}) = \frac{1}{2\pi i}\oint_{S^1_{\rm EP}} dk\cdot\nabla_{\mathbf{k}}\log\det\mathcal{Q}(\mathbf{k}), \tag{8}$$

by $w(\mathbf{k}_{\rm EP}) = -2v_\pm$. The derivation details can be found in Appendix A. Thus, even though EP and its topological invariant are essentially non-Hermitain, it can determine Hermitian phase transition, and such a phase transition is different from conventional ones as shown in Fig. 1(a) by shifting energies.

Let us return to the 1D systems. By treating one of the two dimensions as the parameter to control the phase transition, i.e., γ in Fig. 2(b), the above topological invariant signifies the transition of topological phases in 1D. Because due to topological robustness, the circle $S^1_{\rm EP}$ can be deformed to two loops, L_1 and L_2, as shown in Fig. 2(b). As Eq. (8) is essentially the same as the winding number of Eq. (4), the change of the winding number between L_1 and L_2 equals to the topological invariant of the EP. Thus, surprisingly, we find that non-Hermitian EPs can induce Hermitian topological phase transitions.

V. NON-HERMITIAN BRAIDINGS AND HERMITIAN BULK-BOUNDARY CORRESPONDENCE

According to Hermitian bulk-boundary correspondence, the nontrivial bulk topology corresponds to zero-energy topological boundary states, i.e., $w = n_+^{R(L)} - n_-^{R(L)}$ up to a sign factor. Here, $n_+^{R(L)}$ and $n_-^{R(L)}$ denote the number of zero-energy modes of $|\Psi_+\rangle$ and $|\Psi_-\rangle$ in Eq. (2) that are exponentially localized at the right (left) boundary. Their relation with the bulk nontrivial winding number w is illustrated in Fig. 3.

We have shown that the winding number comes from the non-Hermitian braidings using the linking number of Eq. (5). In one-dimensional non-Hermitian systems, this bulk winding number results in non-Hermitian skin effect (NHSE) [47–51,54], manifested as the localization of wave functions on boundaries. Note that this phenomenon has been observed recently in experiments [52,53]. As the winding number

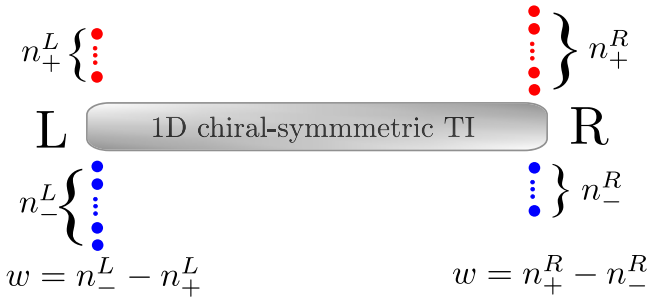

FIG. 3. Hermitian bulk-boundary correspondence in 1D chiral-symmetric topological insulators. The red or blue dots denote zero-energy modes localized at the left or right boundary.

comes from the linking number, we may regard that the NHSE corresponds to the bulk non-Hermitian braidings.

To further establish the relation between non-Hermitian braidings and Hermitian bulk-boundary correspondence, we show that the NHSE in Q gives rise to topological boundary modes in H under semi-infinite boundary conditions (SIBC), following [51,69]. These boundary conditions mean that the system extends to infinite with a single right (left) boundary. Let us consider a non-Hermitian 1D system Q under SIBC. Under this boundary condition, all modes with nontrivial winding number in Q exist and exhibit NHSE [51]. Hence, as we consider the winding number to be nontrivial at the zero energy, i.e., $w \neq 0$ in Eqs. (4) and (5), the zero-energy modes exist and are skin modes under SIBC. We note that the energy of any skin modes can be shifted to zero by adding a reference energy to the system.

The skin modes are exponentially localized at the right (left) boundary described by $\{E_{i,+}, e^{\alpha j}|\psi_{i,+}\rangle\}$ for $Q^\dagger$ and $\{E_{i,-}, e^{\alpha j}|\psi_{i,-}\rangle\}$ for Q. Here, i is the energy index, j the site index, and α the decaying factor. We focus on the zero modes of $Q^\dagger$ and Q, whose numbers are $n_+^{R(L)}$ and $n_-^{R(L)}$, respectively. Here, the superscript R (L) denotes the right (left) boundary of the system under SIBC. In constructing H by Q using Eq. (1), owing to Eq. (3), only these zero-energy modes keep the same localization feature as in Q, while all other modes cannot retain in H [60]. Hence, under SIBC, the topological zero-energy boundary modes in H originate from the zero-energy modes in NHSE of Q, which correspond to the bulk non-Hermitian braidings.

It is noted that in a finite system, instead of SIBC, open boundary conditions (OBC) shall be considered. In this case, the zero-energy skin modes that exist under SIBC may not appear under OBC. However, the relation can still be established by using the concept of pseudospectrum in non-Hermitian systems, as explained in Ref. [69]. Specifically, when these zero-energy modes do not appear under OBC, there would be corresponding modes appearing in the pseudospectrum of Q, which are almost the eigenstates of the system, and they give rise to the topological modes in the Hermitian system.

VI. TYPICAL TOPOLOGICAL PHASES WITH NON-HERMITIAN BRAIDINGS

We now proceed to concrete models that demonstrate how the non-Hermitian braidings give rise to Hermitian topological phases as well as their topological boundary states, whose phase transitions are mediated by critical points. Let us consider a two-band $\mathcal{Q}(k)$ with different non-Hermitian braidings, which has been realized recently [59]. The model Hamiltonian reads as

$$\mathcal{Q}(k) = g\sigma_1 + [\kappa\ \cos k + c\ \cos(2k) + i\Delta\ \sin(2k) - i\gamma]\sigma_3. \tag{9}$$

The two complex-energy eigenvalues are $E(k) = \pm([\kappa\ \cos k + c\ \cos(2k) + i\Delta\ \sin(2k) - i\gamma]^2 + g^2)^{1/2}$.
As shown by I, II, and III in Fig. 4(c) [three green stars in Fig. 4(a)], the braiding of two bands in the $(\mathrm{Re}E(k), \mathrm{Im}E(k), k)$ space leads to different knots (black) in $\mathcal{Q}(k)$. These knots have different linking numbers with the zero-energy loop (red), and thus, they are different phases of $\mathcal{H}(k)$. Specifically, I corresponds to an unlinked phase having

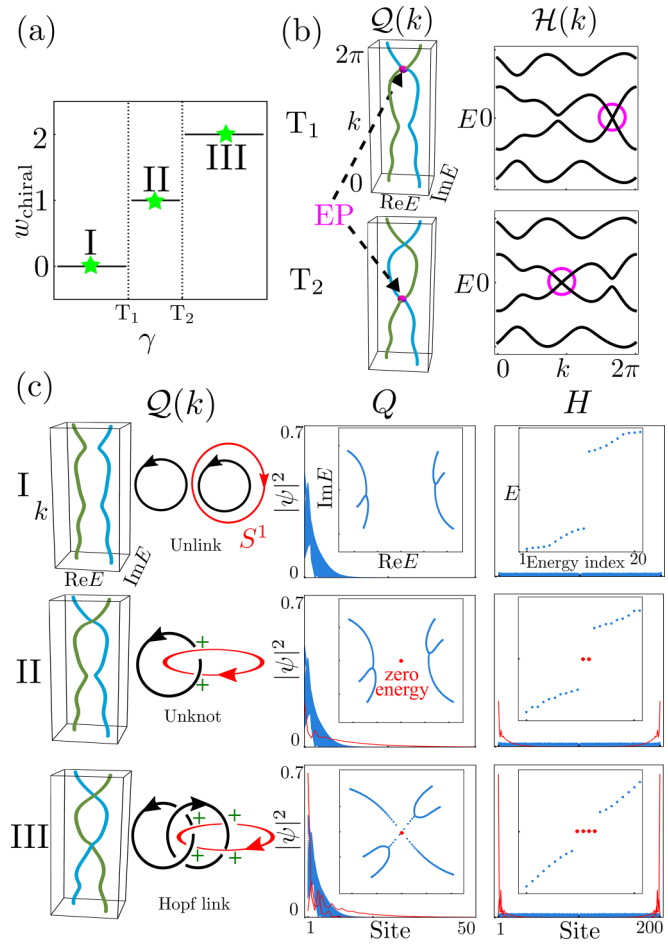

FIG. 4. Typical two-band model. (a) The phase diagram for both $\mathcal{Q}(k)$ and $\mathcal{H}(k)$ against γ. (b) The correspondence between EPs in non-Hermitian $\mathcal{Q}(k)$ and band crossings (open circle) in Hermitian $\mathcal{H}(k)$. (c) The knots of non-Hermitian bands in the 1D BZ (left panel). The wave-function profiles of $\mathcal{Q}(k)$ (middle panel) and $\mathcal{H}(k)$ (right panel) with OBC. The insets in the middle panel shows the complex energy spectra of $\mathcal{Q}(k)$ with OBC. The insets in the right panel show the energy spectra of $\mathcal{H}(k)$ with OBC. The red color refers to zero-energy modes determined by numerical calculations, which belong to the pseudospectrum of $\mathcal{Q}$. The parameters are $\Delta = 0.15$, $g = 3\Delta$, $\kappa = 1.4\Delta$, $c = 1.5\Delta$.

zero linking number; II is an unknot phase with linking number +1; III is a Hopf link phase with linking number +2.

First, we show that the transformation of braiding structure mediated by EPs in $\mathcal{Q}(k)$, as denoted by T_1 and T_2 in Fig. 4(a), leads to Hermitian topological phases transitions in $\mathcal{H}(k)$. Here, $\mathcal{H}(k) = g\sigma_1 \otimes \sigma_1 + [\kappa \cos k + c \cos(2k)]\sigma_1 \otimes \sigma_3 + [\gamma - \Delta \sin(2k)]\sigma_2 \otimes \sigma_3$. We compare the energy spectra of $\mathcal{Q}(k)$ and $\mathcal{H}(k)$ at T_1 and T_2 in Fig. 4(b). The position of band intersection is determined by $E(k) = 0$, as shown by the pink dots in Fig. 4(b). At these points, $\mathcal{Q}(k) = g(\sigma_1 \pm i\sigma_3)$. It is doubly degenerate, but only has one eigenvector of $(\pm i, 1)^T$, corresponding to order-2 EPs. Across these EPs, the winding number changes by +1 due to the change of the non-Hermitian braiding. Thus, the Hermitian phase transitions are determined by these critical points.

Second, we turn to the relation between the non-Hermitian skin modes with zero energy in $\mathcal{Q}$ and the topological boundary states of Hermitian $\mathcal{H}$. In the middle panel of Fig. 4(c), the wave-function profiles of $\mathcal{Q}(k)$ under OBC for I, II, and III phases are plotted, which all possess NHSE. In particular, we numerically calculate the zero-energy states and their wave-function profiles [red points/curves in Fig. 4(c)], which also exhibit skin effects localized at the boundary. However, numerical calculation alone cannot determine whether these are actual zero-energy modes or modes belonging to the pseudospectrum. This is because modes in the pseudospectrum could be very close to actual ones, as the pseudospectrum satisfies [51,69]

$$\sigma_\varepsilon(Q) = \{E \in \mathbb{C} \mid ||(E - Q)|E\rangle|| < \varepsilon\}, \tag{10}$$

where E and $|E\rangle$ represent eigenvalue and eigenstate that are ε close to the actual ones, and numerical calculations of the eigenvalues give only approximate results due to the underlying algorithm. In Appendix B, we demonstrate that these modes belong to the pseudospectrum. Furthermore, we note that in Q, the zero-energy modes themselves are skin modes, not topological boundary modes, as proved in Appendix C. In the right panel of Fig. 4(c), the wave-function profiles for the corresponding $\mathcal{H}(k)$ are plotted under OBC. We can see that only II and III have topological boundary states. This is because for these two, there are zero-energy skin modes in the pseudospectrum of $\mathcal{Q}$, while it is not the case for I. After constructing H by Q, these zero-energy skin modes can give rise to the topological modes.

VII. GENERALIZATION TO MULTIBAND TOPOLOGICAL PHASES WITH HIGHER-ORDER EPs

The mechanism of non-Hermitian braidings can be generalized to multiband models where higher-order EPs (ho EPs) may emerge. Here we discuss the case of triple band $\mathcal{Q}(k)$, where more than two bands could intersect at ho EPs. The non-Hermitian lattice model for $\mathcal{Q}(k)$ reads as

$$\mathcal{Q}(k) = \begin{pmatrix} 0 & \beta & q(k) + \alpha \\ 1 & 0 & 0 \\ 0 & 1 & 0 \end{pmatrix}. \tag{11}$$

Here, $q(k) = \cos k + i \sin k$, and α and β are model parameters. With $\alpha = \beta = 0$, the braiding of the three complex-energy bands forms a knot of circle, as shown in Fig. 5(a).

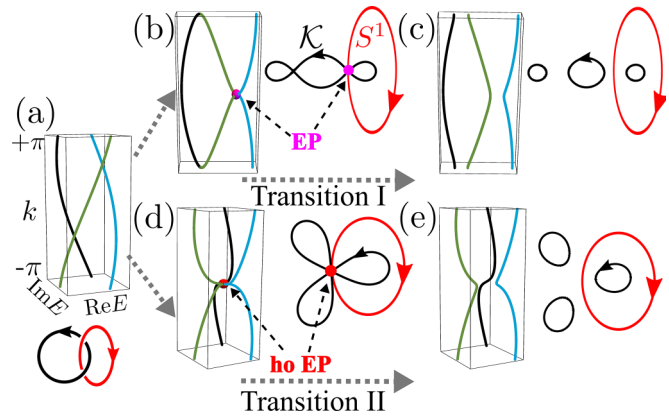

FIG. 5. Generalization to multiband models with higher-order EPs. Transition I of (a) → (b) →(c) is mediated by order-2 EPs. Here $\alpha = 0$, and $\beta = 0$, 1.89, and 2.2. Transition II of (a) → (d) →(e) is mediated by a higher-order EP (ho EP). Here $\beta = 0$, and $\alpha = 0$, −1, and −1.1.

$\mathcal{H}(k)$ possesses a non-trivial phase if zero-energy loop links with this circle.

First, by increasing β, transition I can be induced as shown by Figs. 5(a)–5(c). Similar to Fig. 2, this transition is mediated by order-2 EPs, that is, the intersection of two bands. If one puts the zero-energy loop at such a EP [Fig. 5(b)], the change of knot topology from braiding results in a phase transition. Thus, in multiband cases, order-2 EPs can still lead to topological phase transitions in $\mathcal{H}(k)$.

Second, by decreasing α, transition II can be induced as shown by Figs. 5(a), 5(d), and 5(e). This transition is mediated by ho EP [red point in Figs. 5(d)]. It is different from transition I, as there are three bands intersecting at this point. However, ho EP may also mediate topological phase transition. Because by putting zero-energy loop at this point, transition II also signifies the change of the linking number, resulting the phase transition in $\mathcal{H}(k)$. Therefore, similar to order-2 EPs, ho EP can mediate the change of braiding structure, resulting in the topological phase transitions in $\mathcal{H}(k)$.

VIII. DISCUSSION

We have demonstrated that all the fundamental concepts of chiral-symmetric Hermitian topological phases, including bulk topology, topological phase transition, and bulk-boundary correspondence, have non-Hermitian origins. This non-Hermitian picture provides a deeper understanding which is not possible by Hermitian theories, as signified by the discovery of a class of topological phase transitions characterized by the critical points. Hence, our work shows that non-Hermitian topology may be regarded as building blocks of Hermitian topological phases. In view of the rich concepts in non-Hermitian physics, it would be worthwhile to explore further, e.g., in the following direction. In the case of braiding structures formed by more than two energy bands, similar to the Hermitian systems [70–72], multigap (multiband) conditions may be taken into account. It is expected that partitioning energy gaps and bands into different groups could lead to

different topologies in non-Hermitian Q, which may result in different Hermitian topologies of H.

ACKNOWLEDGMENTS

The authors are grateful to the anonymous referees for their valuable help in this work. This work was supported by the Guangdong-Hong Kong Joint Laboratory of Quantum Matter, the NSFC/RGC JRS grant (Grant No. N_HKU774/21) and the CRF of Hong Kong (Grant No. C6009-20G). W.B.R. was supported by the RGC Postdoctoral Fellowship (Ref. No. PDFS2223-7S05).

APPENDIX A: RELATION BETWEEN VORTICITY AND WINDING NUMBER

In this Appendix, we prove that the topological invariant of order-2 EP, i.e., the vorticity, can determine the change of the winding number. In 2D space, the vorticity of a EP reads as

$$v_{\pm} = -\frac{1}{2\pi}\oint_{S^1_{\rm EP}} dk\cdot\nabla_k \arg\left[E_+(k)-E_-(k)\right]. \tag{A1}$$

Here, k refers to the momentum in the 2D space. The winding number around a EP is

$$w(k_{\rm EP}) = \frac{1}{2\pi i}\oint_{S^1_{\rm EP}} dk\cdot\nabla_k \log\det \mathcal{Q}(k). \tag{A2}$$

The vorticity is a non-Hermitian invariant and takes half-integer values ($\mathbb{Z}/2$) because EP acts as a branch point on the complex-energy plane. In the meantime, the winding number takes integer values.

For the relevant two bands around an order-2 exceptional point (suppose it is located at $k=0$) of $Q(k)$, the effective Hamiltonian can be written as

$$Q_{\rm eff}(k) = d_1(k)\sigma_1 + d_2(k)\sigma_2 + d_3(k)\sigma_3, \tag{A3}$$

where σ_i's ($i=1,2,3$) are Pauli matrices. The energy eigenvalues are

$$E_{\pm}(k) = \pm d(k) = \pm\sqrt{d_1(k)^2+d_2(k)^2+d_3(k)^2}. \tag{A4}$$

The winding number of Eq. (A2) can be calculated as

$$\begin{aligned} w(k_{\rm EP}) &= \frac{1}{2\pi i}\oint_{S^1_{\rm EP}} dk\cdot\nabla_k \log\det Q_{\rm eff}(k)\\ &= \frac{1}{2\pi i}\oint_{S^1_{\rm EP}} dk\cdot\nabla_k \log E_+(k)E_-(k)\\ &= \frac{1}{2\pi i}\oint_{S^1_{\rm EP}} dk\cdot\nabla_k [\log E_+(k)+\log E_-(k)]\\ &= \frac{1}{2\pi i}\oint_{S^1_{\rm EP}} dk\cdot\nabla_k \{\log d(k)+\log[-d(k)]\}. \end{aligned} \tag{A5}$$

The two vorticities ($v_{\pm}$ and $v_{\mp}$) according to Ref. [26] can be calculated as

$$\begin{aligned} v_{\pm} &= -\frac{1}{2\pi}\oint_{S^1_{\rm EP}} dk\cdot\nabla_k \arg[E_+(k)-E_-(k)]\\ &= -\frac{1}{2\pi}\oint_{S^1_{\rm EP}} dk\cdot\nabla_k \arg[2d(k)]\\ &= -\frac{1}{2\pi}\oint_{S^1_{\rm EP}} dk\cdot\nabla_k \left(-i\,\log\frac{2d(k)}{|2d(k)|}\right)\\ &= -\frac{1}{2\pi i}\oint_{S^1_{\rm EP}} dk\cdot\nabla_k \log d(k). \end{aligned} \tag{A6}$$

Note we use the facts that $\arg(z) = -i\,\log(\frac{z}{|z|})$ in the third step and that $|\log d(k)|$ is a single-valued function in the last step. And similarly,

$$\begin{aligned} v_{\mp} &= -\frac{1}{2\pi}\oint_{S^1_{\rm EP}} dk\cdot\nabla_k \arg[E_-(k)-E_+(k)]\\ &= -\frac{1}{2\pi}\oint_{S^1_{\rm EP}} dk\cdot\nabla_k \arg[-2d(k)]\\ &= -\frac{1}{2\pi i}\oint_{S^1_{\rm EP}} dk\cdot\nabla_k \log[-d(k)]. \end{aligned} \tag{A7}$$

In view of the winding number $w(k_{\rm EP})$ of Eq. (A5) and the vorticities ($v_{\pm}$ and $v_{\mp}$) of Eqs. (A6) and (A7), it is clear that

$$w(k_{\rm EP}) = -(v_{\pm}+v_{\mp}). \tag{A8}$$

We note that $v_{\pm}$=$v_{\mp}$ because

$$\begin{aligned} v_{\mp} &= -\frac{1}{2\pi i}\oint_{S^1_{\rm EP}} dk\cdot\nabla_k \arg[-2d(k)]\\ &= -\frac{1}{2\pi i}\oint_{S^1_{\rm EP}} dk\cdot\nabla_k \big(\arg[2d(k)]+\pi\big)\\ &= -\frac{1}{2\pi i}\oint_{S^1_{\rm EP}} dk\cdot\nabla_k \big(\arg[2d(k)]\big)\\ &= v_{\pm}. \end{aligned} \tag{A9}$$

Thus, we have

$$w(k_{\rm EP}) = -2v_{\pm}\ (\text{or}\ -2v_{\mp}). \tag{A10}$$

Therefore, the winding number of $w(k_{\rm EP})$ is determined by the vorticity of exceptional point. While the vorticities take half-integer values, the winding number takes integer values. This is different from the ordinary phase transition by shifting energies.

APPENDIX B: ZERO-ENERGY MODES IN FIG. 4(c) BELONG TO PSEUDOSPECTRUM

In this Appendix, we demonstrate that the zero-energy modes in Fig. 4(c) II, obtained numerically by diagonalizing the Hamiltonian, belong to the pseudospectrum.

First, we investigate the behavior around the phase transition point T_1 in Fig. 4. As shown in Fig. 6, we calculate the spectra immediately before T_1, i.e., $T_1-0.01$, and immediately after T_1, i.e., $T_1+0.01$. We find that there exists a zero mode $|0\rangle$ satisfying,

$$||Q|0\rangle|| < 10^{-4} \tag{B1}$$

at $T_1+0.01$, while there is no such mode at $T_1-0.01$. Note that numerical calculations give only approximate values, which means this mode may also belong to pseudospectrum according to Eq. (10). To determine whether this is an actual zero mode of Q, we note that the phase transition is tuned by a continuous parameter γ and, thus, the spectrum shall change

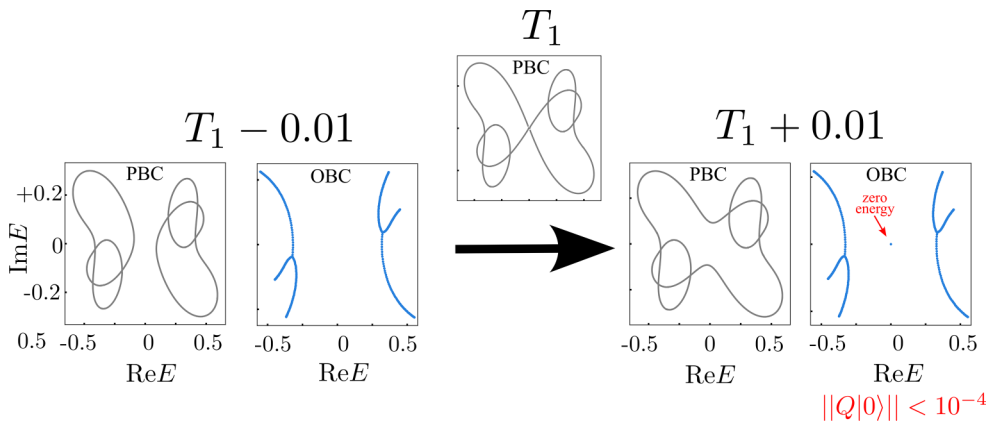

FIG. 6. The evolution of the PBC and OBC spectra around the phase transition point at T_1. Numerical calculation shows that the zero modes appear immediately after T_1, determined by the criteria $||Q|0\rangle|| < 10^{-4}$.

continuously. Hence, if zero modes exist after T_1, some modes shall approach zero before T_1. However, there are no such modes at $T_1 - 0.01$. Thus, by the continuous property of the Hamiltonian, this isolated zero mode shall not be an actual mode of Q.

Second, having ruled out the zero modes of Eq. (B1) as actual zero modes of Q, we proceed to demonstrate that this zero mode belongs to the pseudospectrum. According to Refs. [51,69], the pseudospectrum satisfies

$$\lim_{\epsilon\to 0}\lim_{N\to\infty}\sigma_\epsilon(Q_{\mathrm{OBC}}) = \sigma(Q_{\mathrm{SIBC}}), \tag{B2}$$

where N is the system size, and Q_{OBC} and Q_{SIBC} are the Hamiltonians of OBC and SIBC systems, respectively. The above equation means that after taking the limits, the pseudospectrum $\sigma_\epsilon(Q_{\mathrm{OBC}})$ is equal to the SIBC spectrum $\sigma(Q_{\mathrm{SIBC}})$, which is given by the union of $\sigma(Q_{\mathrm{PBC}})$ and the whole area of $E \in \mathbb{C}$ enclosed by $\sigma(Q_{\mathrm{PBC}})$ with a nonzero spectral winding number. Here, $\sigma(Q_{\mathrm{PBC}})$ refers to the PBC spectrum. Regarding the region immediately after T_1, as shown in Fig. 6, for a fixed ε with a large N, the pseudospectrum is given by the region enclosed by the PBC spectrum with nonzero winding number, which includes the zero-energy point and differs from the region immediately before T_1. Thus, after T_1, the zero mode can appear in this pseudospectrum region, which is determined by $\varepsilon = 10^{-4}$ of Eq. (B1) in numerical calculations.

APPENDIX C: ZERO-ENERGY MODES IN FIG. 4(c) ARE NOT TOPOLOGICAL MODES IN Q

In this Appendix, we further demonstrate that the zero-energy modes in Fig. 4(c) II and III in the main text are skin modes, not topological modes of Q. To do this, we first show that these modes have the common feature of skin modes, and then show that other than non-Hermitian braidings, there is no additional nontrivial topological structure associated with the model Hamiltonian of Eq. (9) in the main text.

First, the skin modes have the common feature of appearing inside the periodic boundary spectrum. This is because they have a nontrivial winding number, which requires to be enclosed by the periodic boundary spectrum. In Fig. 7, we plot the spectra of $Q(k)$ for I, II, and III under periodic boundary condition (PBC), corresponding to Fig. 4(c) in the main text, and then compare them with those under open boundary condition (OBC). We can see that the OBC spectra (blue) all fall inside the PBC spectrum (gray) for I, II, and III. In particular, for the zero modes of OBC in II and III, as highlighted by red arrows, they also fall inside the PBC spectrum (gray). Thus, these zero modes have the feature of skin modes.

Second, the above criteria, however, cannot fully rule out the possibility that these zero-energy modes are topological modes. Because there is a special chiral symmetry σ_y for $Q(k)$ of Eq. (8) in the main text, to achieve the goal of ruling out topological modes, we need to calculate the winding number (denoted as w_2) associated with this special chiral symmetry σ_y. A nontrivial w_2 indicates the existence of topological zero modes, while a trivial one cannot. However, since $Q(k)$ is non-Hermitian, we cannot directly calculate w_2 using the Bloch Hamiltonian because of the difference between PBC and OBC spectrum. Following Refs. [46,47] in the main text, we use the non-Bloch band theory and calculate the generalized Brillouin zone (GBZ) first, and then use the GBZ to compute the non-Bloch topological invariant w_2.

In Fig. 8(a), the GBZ for Fig. 4(c) I in the main text is obtained, which corresponds to Fig. 7 I above. We use this GBZ to compute the band spectrum E_{GBZ} and plot it in Fig. 8(b). Comparing with OBC spectrum E_{OBC}, we can see that GBZ can well predict the behavior of open boundary systems.

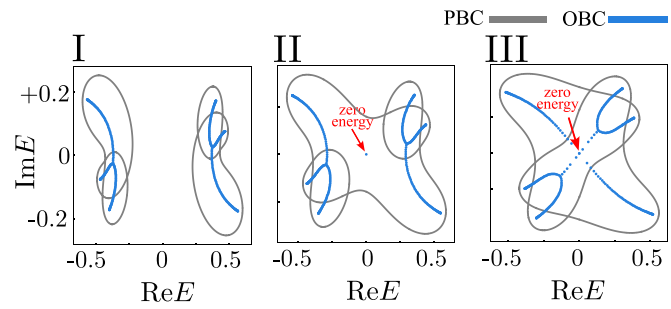

FIG. 7. The comparison between spectra under periodic boundary condition (PBC, gray) and open boundary condition (OBC, blue). The zero modes in OBC spectra are highlighted by red arrows, which fall inside the PBC spectra.

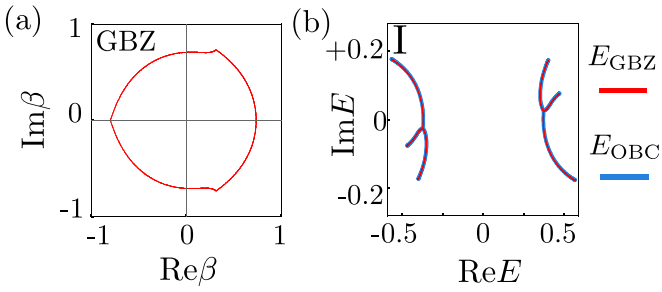

FIG. 8. (a) Generalized Brillouin zone (GBZ) calculated for Fig. 4(c) I in the main text. (b) The comparison between the GBZ spectrum $E_{\rm GBZ}$ and the OBC spectrum $E_{\rm OBC}$.

We proceed to compute the non-Bloch winding number w_2 based on GBZ. First, we perform a unitary transformation $U = \exp(i\frac{\pi}{4}\sigma_x)$ to obtain the standard off-diagonal form of $Q(k)$,

$$UQ(k)U^{-1} = \begin{pmatrix} 0 & R_+(\beta) \\ R_-(\beta) & 0 \end{pmatrix}, \tag{C1}$$

where the chiral symmetry operator becomes $U\sigma_y U^{-1} = -\sigma_z$. Note that we have substituted k with β for GBZ ($k \to \beta = e^k$). Then, according to Eq. (8) of Ref. [47] in the main text, the winding number w_2 can be computed as

$$w_2 = -\frac{w_+ - w_-}{2}, \quad w_\pm = \frac{1}{2\pi}[\arg\ R_\pm(\beta)]_{C_\beta}, \tag{C2}$$

where $[\arg\ R_\pm(\beta)]_{C_\beta}$ means the change of phase of $R_\pm(\beta)$ as β goes along the generalized Brillouin zone C_β in a counterclockwise way.

As shown in Fig. 9 above, we have calculated the non-Bloch winding number w_2 numerically. We find that it is trivial, i.e., $w_2 = 0$, for all γ in the range same as Fig. 4(a) in the main text. In particular, for the parameters of I, II, and III in Fig. 4(c) (or Fig. 7 above), their winding numbers are all trivial ($w_2 = 0$). Therefore, we can conclude that the zero modes in II and III are not topological modes. In other words, they are skin modes.

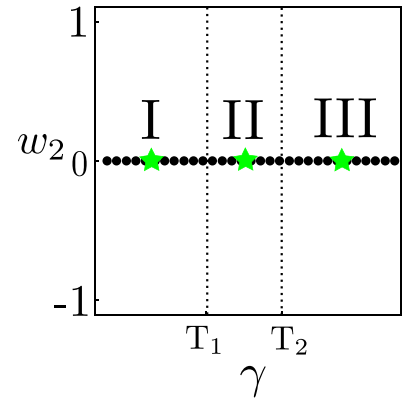

FIG. 9. The non-Bloch winding number calculated by the generalized Brillouin zone (GBZ). It corresponds to the special chiral symmetry of the non-Hermitian $Q(k)$. The plot range is the same as Fig. 4(a) in the main text.

APPENDIX D: AN EXAMPLE OUTSIDE CLASS AIII

In the main text, we consider H in Hermitian class AIII constructed by Q using Eq. (1). In this Appendix, we provide an example outside class AIII, namely, a model in class BDI.

The momentum-space Hamiltonian reads as

$$Q(k) = g\sigma_1 + [c\ \sin(2k) + ic\ \cos(2k) - i\gamma]\sigma_3, \tag{D1}$$

where g, c, and γ are model parameters, and σ_i's are standard Pauli matrix. Here, $Q(k)$ has a similar braiding topology as that in Fig. 4(c) III, for parameters $c = 0.15$, $g = 0.2$, and $\gamma = 0.2$.

Based on $Q(k)$, we can construct the Hermitian Hamiltonian

$$H(k) = g\tau_1 \otimes \sigma_1 + c\ \sin(2k)\tau_1 \otimes \sigma_3 - [c\ \cos(2k) - \gamma]\tau_2 \otimes \sigma_3. \tag{D2}$$

Aside from chiral symmetry, this Hamiltonian has the following symmetries: (i) charge-conjugation symmetry

$$CH(k)C^{-1} = -H(-k), \qquad C = \tau_0 \otimes \sigma_3\mathcal{K}, \tag{D3}$$

and (ii) time-reversal symmetry

$$TH(k)T^{-1} = H(-k), \qquad T = \tau_0 \otimes \sigma_1\mathcal{K}. \tag{D4}$$

Here $\mathcal{K}$ is the complex-conjugation operation. Because $C^2 = T^2 = +1$, the model Hamiltonian belongs to class BDI. It is straightforward to verify that $H(k)$ has a nontrivial topology due to the braiding in $Q(k)$.

[1] J. M. Leinaas and J. Myrheim, Nuovo Cimento B **37**, 1 (1977).
[2] F. Wilczek, Phys. Rev. Lett. **48**, 1144 (1982).
[3] C. Nayak, S. H. Simon, A. Stern, M. Freedman, and S. Das Sarma, Rev. Mod. Phys. **80**, 1083 (2008).
[4] Q. Wu, A. A. Soluyanov, and T. Bzdusek, Science **365**, 1273 (2019).
[5] E. Yang, B. Yang, O. You, H.-C. Chan, P. Mao, Q. Guo, S. Ma, L. Xia, D. Fan, Y. Xiang, and S. Zhang, Phys. Rev. Lett. **125**, 033901 (2020).
[6] D. Wang, B. Yang, Q. Guo, R.-Y. Zhang, L. Xia, X. Su, W.-J. Chen, J. Han, S. Zhang, and C. T. Chan, Light Sci. Appl. **10**, 83 (2021).
[7] H. Park, S. Wong, X. Zhang, and S. S. Oh, ACS Photonics **8**, 2746 (2021).
[8] A. Bouhon, Q. Wu, R.-J. Slager, H. Weng, O. V. Yazyev, and T. Bzdusek, Nat. Phys. **16**, 1137 (2020).
[9] Q. Guo, T. Jiang, R.-Y. Zhang, L. Zhang, Z.-Q. Zhang, B. Yang, S. Zhang, and C. T. Chan, Nature (London) **594**, 195 (2021).

[10] B. Jiang, A. Bouhon, Z.-K. Lin, X. Zhou, B. Hou, F. Li, R.-J. Slager, and J.-H. Jiang, Nat. Phys. **17**, 1239 (2021).

[11] B. Peng, A. Bouhon, B. Monserrat, and R.-J. Slager, Nat. Commun. **13**, 423 (2022).

[12] Z. Yang, C.-K. Chiu, C. Fang, and J. Hu, Phys. Rev. Lett. **124**, 186402 (2020).

[13] W. Tang, X. Jiang, K. Ding, Y.-X. Xiao, Z.-Q. Zhang, C. T. Chan, and G. Ma, Science **370**, 1077 (2020).

[14] K. Wang, L. Xiao, J. C. Budich, W. Yi, and P. Xue, Phys. Rev. Lett. **127**, 026404 (2021).

[15] W. Tang, K. Ding, and G. Ma, Nat. Sci. Rev. **9**, nwac010 (2022).

[16] D.-L. Deng, S.-T. Wang, C. Shen, and L.-M. Duan, Phys. Rev. B **88**, 201105(R) (2013).

[17] T. Bzdušek and M. Sigrist, Phys. Rev. B **96**, 155105 (2017).

[18] J. Ahn, D. Kim, Y. Kim, and B.-J. Yang, Phys. Rev. Lett. **121**, 106403 (2018).

[19] K. Wang, J.-X. Dai, L. B. Shao, S. A. Yang, and Y. X. Zhao, Phys. Rev. Lett. **125**, 126403 (2020).

[20] K. Esaki, M. Sato, K. Hasebe, and M. Kohmoto, Phys. Rev. B **84**, 205128 (2011).

[21] D. Leykam, K. Y. Bliokh, C. Huang, Y. D. Chong, and F. Nori, Phys. Rev. Lett. **118**, 040401 (2017).

[22] Y. Xiong, J. Phys. Commun. **2**, 035043 (2018).

[23] H. Menke and M. M. Hirschmann, Phys. Rev. B **95**, 174506 (2017).

[24] Y. Xu, S.-T. Wang, and L.-M. Duan, Phys. Rev. Lett. **118**, 045701 (2017).

[25] T. E. Lee, Phys. Rev. Lett. **116**, 133903 (2016).

[26] H. Shen, B. Zhen, and L. Fu, Phys. Rev. Lett. **120**, 146402 (2018).

[27] H. Zhou, C. Peng, Y. Yoon, C. W. Hsu, K. A. Nelson, L. Fu, J. D. Joannopoulos, M. Soljačić, and B. Zhen, Science **359**, 1009 (2018).

[28] W. B. Rui, Z. Zheng, M. M. Hirschmann, S.-B. Zhang, C. Wang, and Z. D. Wang, npj Quantum Mater. **7**, 15 (2022).

[29] J. Hou, Z. Li, X.-W. Luo, Q. Gu, and C. Zhang, Phys. Rev. Lett. **124**, 073603 (2020).

[30] Z. Gong, Y. Ashida, K. Kawabata, K. Takasan, S. Higashikawa, and M. Ueda, Phys. Rev. X **8**, 031079 (2018).

[31] W. B. Rui, M. M. Hirschmann, and A. P. Schnyder, Phys. Rev. B **100**, 245116 (2019).

[32] K. Kawabata, K. Shiozaki, M. Ueda, and M. Sato, Phys. Rev. X **9**, 041015 (2019).

[33] L. Li, C. H. Lee, and J. Gong, Phys. Rev. B **100**, 075403 (2019).

[34] E. J. Bergholtz, J. C. Budich, and F. K. Kunst, Rev. Mod. Phys. **93**, 015005 (2021).

[35] M. Berry, Czech. J. Phys. **54**, 1039 (2004).

[36] W. D. Heiss, J. Phys. A: Math. Theor. **45**, 444016 (2012).

[37] M.-A. Miri and A. Alu, Science **363**, eaar7709 (2019).

[38] T. Kato, in *Perturbation Theory for Linear Operators*, Classics in Mathematics, edited by T. Kato (Springer, Berlin, 1995), pp. 62–126.

[39] K. Kawabata, T. Bessho, and M. Sato, Phys. Rev. Lett. **123**, 066405 (2019).

[40] W. B. Rui, Y. X. Zhao, and A. P. Schnyder, Phys. Rev. B **99**, 241110(R) (2019).

[41] D. Bernard and A. LeClair, in *Statistical Field Theories*, NATO Science Series, edited by A. Cappelli and G. Mussardo (Springer, Dordrecht, 2002), pp. 207–214.

[42] H. Zhou and J. Y. Lee, Phys. Rev. B **99**, 235112 (2019).

[43] S. Lieu, Phys. Rev. B **98**, 115135 (2018).

[44] J. C. Budich, J. Carlström, F. K. Kunst, and E. J. Bergholtz, Phys. Rev. B **99**, 041406(R) (2019).

[45] W. B. Rui, Z. Zheng, C. Wang, and Z. D. Wang, Phys. Rev. Lett. **128**, 226401 (2022).

[46] C. H. Lee and R. Thomale, Phys. Rev. B **99**, 201103(R) (2019).

[47] F. K. Kunst, E. Edvardsson, J. C. Budich, and E. J. Bergholtz, Phys. Rev. Lett. **121**, 026808 (2018).

[48] S. Yao and Z. Wang, Phys. Rev. Lett. **121**, 086803 (2018).

[49] K. Yokomizo and S. Murakami, Phys. Rev. Lett. **123**, 066404 (2019).

[50] K. Zhang, Z. Yang, and C. Fang, Phys. Rev. Lett. **125**, 126402 (2020).

[51] N. Okuma, K. Kawabata, K. Shiozaki, and M. Sato, Phys. Rev. Lett. **124**, 086801 (2020).

[52] L. Xiao, T. Deng, K. Wang, G. Zhu, Z. Wang, W. Yi, and P. Xue, Nat. Phys. **16**, 761 (2020).

[53] T. Helbig, T. Hofmann, S. Imhof, M. Abdelghany, T. Kiessling, L. W. Molenkamp, C. H. Lee, A. Szameit, M. Greiter, and R. Thomale, Nat. Phys. **16**, 747 (2020).

[54] D. S. Borgnia, A. J. Kruchkov, and R.-J. Slager, Phys. Rev. Lett. **124**, 056802 (2020).

[55] Z. Li and R. S. K. Mong, Phys. Rev. B **103**, 155129 (2021).

[56] C. C. Wojcik, X.-Q. Sun, T. Bzdušek, and S. Fan, Phys. Rev. B **101**, 205417 (2020).

[57] H. Hu and E. Zhao, Phys. Rev. Lett. **126**, 010401 (2021).

[58] H. Hu, S. Sun, and S. Chen, Phys. Rev. Res. **4**, L022064 (2022).

[59] K. Wang, A. Dutt, C. C. Wojcik, and S. Fan, Nature (London) **598**, 59 (2021).

[60] Away from zero energy, the eigenequation can also be obtained by the non-Hermitian components Q and $Q^\dagger$, i.e., $Q\psi_- = E\psi_+$ and $Q^\dagger\psi_+ = E\psi_-$, which yield $QQ^\dagger\psi_+ = E^2\psi_+$, $Q^\dagger Q\psi_- = E^2\psi_-$. However, this becomes a coupled eigenvalue problem, and the information from either Q or $Q^\dagger$ alone cannot be retained in the Hermitian Hamiltonian H.

[61] C.-K. Chiu, J. C. Y. Teo, A. P. Schnyder, and S. Ryu, Rev. Mod. Phys. **88**, 035005 (2016).

[62] A. J. Heeger, S. Kivelson, J. R. Schrieffer, and W. P. Su, Rev. Mod. Phys. **60**, 781 (1988).

[63] J. K. Asbóth, L. Oroszlány, and A. Pályi, in *A Short Course on Topological Insulators: Band Structure and Edge States in One and Two Dimensions*, Lecture Notes in Physics, edited by J. K. Asbóth, L. Oroszlány, and A. Pályi (Springer, Cham, 2016), pp. 1–22.

[64] R. Roy and F. Harper, Phys. Rev. B **96**, 155118 (2017).

[65] J. Y. Lee, J. Ahn, H. Zhou, and A. Vishwanath, Phys. Rev. Lett. **123**, 206404 (2019).

[66] Given non-Hermitian Q_1 and Q_2, they have the same point-gap topology about a reference point E_P on the complex-energy plane, if their spectra can be smoothly deformed to each other without crossing E_P.

[67] Here, the simplification refers to the comparison between integration and counting crossings. There might be another computational cost arising in calculating the linking number. That is, to obtain the linking number, it is required to identify

all the eigenvalues, while in Eq. (4) only the computation of the determinant is required.

[68] Z. Yang, A. P. Schnyder, J. Hu, and C.-K. Chiu, Phys. Rev. Lett. **126**, 086401 (2021).

[69] N. Okuma and M. Sato, Phys. Rev. B **102**, 014203 (2020).

[70] A. Bouhon, T. Bzdušek, and R.-J. Slager, Phys. Rev. B **102**, 115135 (2020).

[71] F. N. Ünal, A. Bouhon, and R.-J. Slager, Phys. Rev. Lett. **125**, 053601 (2020).

[72] A. Bouhon and R.-J. Slager, arXiv:2203.16741.